On the Coupling Mechanism of Equiaxed Crystal Generation with the Liquid Flow Driven by Natural Convection During Solidification

MIHAELA STEFAN-KHARICHA, ABDELLAH KHARICHA, MENGHUAI WU, and ANDREAS LUDWIG

The influence of the melt flow on the solidification structure is bilateral. The flow plays an important role in the solidification pattern, *via* the heat transfer, grain distribution, and segregations. On the other hand, the crystal structure, columnar or equiaxed, impacts the flow, *via* the thermosolutal convection, the drag force applied by the crystals on the melt flow, *etc*. As the aim of this research was to further explore the solidification–flow interaction, experiments were conducted in a cast cell (95 * 95 * 30 mm^3), in which an ammonium chloride–water solution (between 27 and 31 wt pct NH_4Cl) was observed as it solidified. The kinetic energy (KE) of the flow and the average flow velocity were calculated throughout the process. Measurements of the volume extension of the mush in the cell and the velocity of the solid front were also taken during the solidification experiment. During the mainly columnar experiments (8 cm liquid height) the flow KE continuously decreased over time. However, during the later series of experiments at higher liquid height (9.5 cm), the flow KE evolution presented a strong peak shortly after the start of solidification. This increase in the total flow KE correlated with the presence of falling equiaxed crystals. Generally, a clear correlation between the strength of the flow and the occurrence of equiaxed crystals was evident. The analysis of the results strongly suggests a fragmentation origin of equiaxed crystals appearing in the melt. The transition from purely columnar growth to a strongly equiaxed rain (CET) was found to be triggered by (a) the magnitude of the coupling between the flow intensity driven by the equiaxed crystals, and (b) the release and transport of the fragments by the same flow recirculating within the mushy zone.

Graphical Abstract

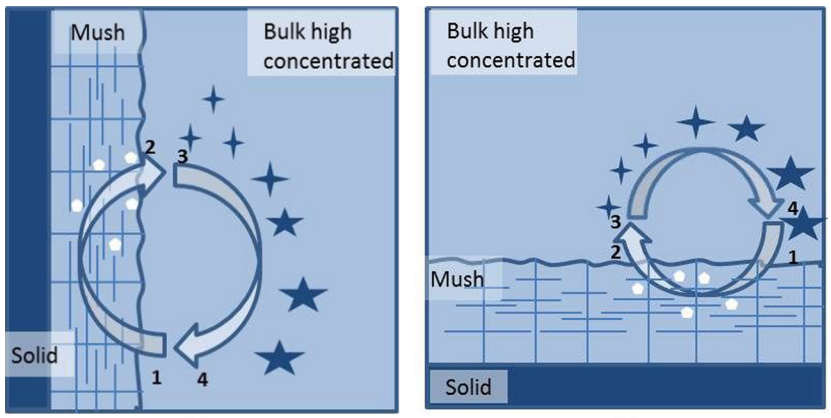

MIHAELA STEFAN-KHARICHA, ABDELLAH KHARICHA, MENGHUAI WU, and ANDREAS LUDWIG are with the Department of Metallurgy, Montanuniversitaet Leoben, Franz-Josef-Str. 18, 8700 Leoben, Austria. Contact e-mail: mihaela.stefan-kharicha@unileoben.ac.at

Manuscript submitted February 3, 2017.
Article published online February 14, 2018

Coupling mechanism at the origin of CET: 1-2 strong flow running through the mush transporting out dendrite fragments (white dots); 3-4 equiaxed growth and drag of the downward flow. If the vortex is sufficiently stable, the horizontal configuration can lead to freckle appearing; a) vertical solidification front; b) horizontal solidification front.

https://doi.org/10.1007/s11661-018-4489-3

I. INTRODUCTION

THE mechanism of how equiaxed grains originate can be explained by two theories: heterogeneous nucleation or fragmentation. The nucleation consists primarily in the creation of nuclei, and secondly, their growth. When the temperature falls below the melting temperature, low enough that an interface between solid and liquid can be created, a nucleus is formed. Most nucleation models postulate that nucleation is a thermally activated process.[1] Once the nucleus reaches the critical size R_c, it can continue to grow. The decreasing atoms' mobility at reduced temperatures contributes to the nucleation rate *via* the atomic variation frequency and the probability of capturing a new atom. The nucleation rate increases rapidly with rising undercooling. In the nucleation mechanism of equiaxed crystal formation, the flow plays an important role during the crystal growth, but is of no significance in nuclei creation phase. Through its interaction with the thermosolutal field, the flow impacts the size of the undercooled region, which needs to be sufficiently large to allow equiaxed crystal growth. In addition, flow also controls the transport of the nuclei.

The generation of equiaxed crystals by fragmentation inside the mushy zone entails the fulfillment of three conditions. First the production of dendrite's fragments in the mushy zone should take place. Secondly, a flow strong enough to penetrate the mush and carry these dendrite fragments in the bulk. The transformation of the fragments into equiaxed crystals is the last condition, *i.e.*, the existence of a sufficiently large undercooled region ahead of the columnar front.

Dendrite fragmentation could occur for different reasons and in many circumstances. Paradies *et al.*[2] performed experiments under forced flow convection (around 10 cm s^{-1}) in superheated SCN—acetone melt, under different system parameters (cooling rate, temperature difference between the chill walls, melt flow rate). The fragmentation rate (number of fragments counted per mm^2 and per second) correlated with a higher velocity melt near the mushy zone. Small fragments less than 0.2 mm were used to measure the velocity melt near the mushy region (0.2 mm beyond the longest dendrite and 0.4 mm into the mushy region). The increase in fragmentation rate correlated with the direction of the flow near the mushy zone, and observations showed that downward flow induced less of an increase than the upward flow near the mushy region. However, it was not possible to deduce a clear relation between the observed fragmentation rate and the controlling parameters of the system. The mechanism at the origin of fragmentation was unclear, but assumedly it was rather due to remelting or capillary pinching than mechanical shear, even if hydrodynamic shear could not be totally excluded.

Remelting of high-order (secondary and tertiary) trunk dendrites originates at the root branches, where the curvature comparing with the tip is larger. Undercooling is a pre-requisite in order to achieve solidification. The dendrite tip curvature during solidification drops as the undercooling rises, thus the greater the extent of undercooling, the faster solid growth occurs. Local changes in the solute concentration in the columnar mush can cause remelting of secondary or tertiary dendrite arms. Pileup of solute in the mush, caused by melt flow or variations in the grow velocity of the columnar front, are possible sources of interdendritic solute variations. Recalescence due to interdendritic melt solidification will raise the temperature and remelt dendrite branches. Jackson *et al.*[3] was the first to suggest that remelting was the mechanism of dendrite detachment due to local undercooling and solute concentration variations in the mushy zone. Equally, the forced convection due to electromagnetic stirring can cause dendrite fragmentation as found by Campanella *et al.*[4] in copper-base alloys. The fragmentation rate was found to be higher if the magnetic field is stronger, if the distance between the coil and the liquid–solid interface is shorter (the induced flow vortices are close to the dendrite tips and able to enter the mushy zone), and if the alloy is more permeable. In addition, a simple fragmentation criterion was found, based on Fleming's analysis of mushy zone remelting.[5] This indicates that a distance equal to $8\lambda_2$ (λ_2 being the final secondary dendrite arm spacing) is necessary to render fragmentation; otherwise only dendrite remelting takes place. Experiments in a modified Bridgman furnace (with an induced coil) on two copper-base alloys confirmed the numerical model based on the fragmentation criterion. A higher concentration alloy is more permeable and leads to finer grains.

Dragnevski *et al.*[6] presented a numerical flow model for dendritic solidification of strongly undercooled melt (50 K to 100 K), when both conditions for dendrite bending, high flow velocities and very fine dendrites, exist. They use a more realistic geometrical model than the analytical model of Pilling and Hellawell,[7] where the dendrites were modeled as cylinders. The results obtained with the two models, for the bending moment function of the flow Reynolds number, are in good

agreement. It was also proved experimentally that mechanical deformation can take place when the dendrite tip radius reaches a local minimum.

The scale of the scenery, where these fragmentation phenomena take place, is microscopic, hence it is difficult to distinguish between them. *In situ* observations were performed with X-ray microscopy[8] on the crystal fragmentation in an Al-Cu alloy. Experimental observations demonstrate that detachment always occurs on the tertiary branches first and sometimes a secondary-arm fragmentation can happen as a consequence of initial fragmentation. They prove that high-order side-branch remelting is prone to producing dendrite fragmentation as opposed to coarser parent branches. In conclusion, fragmentation rate depends on the degree of network branching.

Dendrite fragmentation can occur as a result of coarsening mechanisms or recalescence.[3] However, these phenomena occur deep in the mush and the transport and survival chance of detached dendrites through the low permeable mush is unpredictable. Remelting of tertiary branches at the root to the parent dendrite remains a better pathway for dendrite detachment. Previous to the dendrite fragmentation by remelting, a minor deceleration[9] of the columnar front velocity is noticeable. Ruvalcaba *et al*. hypothesized that this deceleration would induce enhancement of solute at the columnar front and subsequently the solute-rich liquid will settle into the mush and initiate dendrite detachment. The time it takes for a dendrite to detach was measured to be in the range of a few seconds.

Beckermann[10] presents a summary of experimental and numerical works on the convective transport of a single equiaxed crystal at the large scale of a casting. It is crucial to estimate the relative velocity between the settling crystal and the melt flow in convection cases. In this order, the drag force between the equiaxed grain and the melt plays a highly significant role. If the equiaxed grain is globular, Stoke's law applies, and if the grain has a dendritic structure Darcy's law is used to calculate the drag force. The dendrite tip speed can be one order of magnitude higher in the presence of convective flow than in the diffusion case. The solid phase transport is expected to reduce the macrosegregation in this system.

Kumar and Dutta[11] also took into account that dendrite fragmentation may occur as a consequence of local dendrite remelting near the dendrite stem. They tried to quantify a Rayleigh number based on a dendrite fragmentation criterion. The fragmentation criterion merely depends on the concentration difference, liquid fraction, permeability of the mush, grow rate of the mushy zone, and thermophysical parameters. A critical Rayleigh number equal to 1 was found to be necessary in order to induce remelting and subsequent fragmentation. For the same concentration difference, a more permeable mush is more likely to produce remelting and fragmentation. There is a lower probability for remelting and fragmentation in the mush with a faster solidification rate for a given concentration difference.

Montgomery and Incropera[12] studied experimentally the direct solidification of hypereutectic ammonium chloride alloys cooled by bellows (vertical direct solidification, VDS) or by the side wall (horizontal direct solidification, HDS). The fragments produced were counted in a delimited area. The number was found to increase with an increase of initial NH_4Cl concentration in the case of VDS. In contrast, the number rose with a decreasing initial ammonium chloride concentration, in the case of HDS. Moreover, the temperature of the chill plate was varied and the number and size of fragments increased in both cases with decreasing chill wall temperature. In both cases (VDS and HDS), several stages are presumed to exist in the fragment's production. The most important are: (a) remelting, due to latent heat release or drop of liquidus temperature (because of the water-rich interdendritic liquid) and (b) fragmentation in channels, due to strong flow or remelting in the upper region (where water-rich cells developed).

In order to better understand CET, Gandin[13] developed a one-dimensional model based on the interaction of the heat flow at the dendritic interface and the columnar front. When the maximum columnar front velocity was reached and the thermal gradient ahead in the liquid became negative, CET took place. Consequently, fragmentation by dendrite arm remelting and destabilization of the columnar dendritic interface are considered as a hypothesis for the CET. Comparison of simulation results with Al-Si solidification experiments showed good agreement.

The model for the columnar-to-equiaxed transition (CET) proposed by Martorano *et al*.[14] is based on the strong interactions of solutal undercooling and respectively solutal buoyancy, between the columnar front and the equiaxed crystals. Solutally driven flow is crucial in alloys where the rejected solute is lighter (as in hypereutectic ammonium chloride alloys). It was noticed that an increase in the columnar front velocity stimulated equiaxed solidification. The assumption that the CET is the result of the fragmentation of dendrites was emitted.

Hunt[15] considered the growth of equiaxed crystals ahead of a columnar front in his model. In his analysis, he used a simple relation between the velocity columnar front and the square of undercooling and took into account the solute rejection at the dendrite tip. Browne,[16] in his approach of columnar growth, considered the same expression developed by Hunt and he suggested that equiaxed solidification is more probable in alloys with high solute concentrations and where the heat transfer is low.

A great deal of work was conducted by Sivarupan *et al*.[17] on different Al-Si-Cu-Mg-Fe/Mn alloys. For a given composition a relationship between the cooling rate and the SDAS (secondary dendrite arm spacing) was found, in the form of $\lambda_2 = aR^{-n}$, where a and n are alloy-dependent constants, which vary with composition and cooling rate and R is the relation between the average cooling rate and the solidification time.

For peritectic directional solidification, a model was developed[18] in order to evaluate the secondary-arm spacing after coarsening. The model proposes three stages for the thin arm dissolution (thick-arm coarsening). The calculations show that $\lambda_2 V^m$ is constant for a

given alloy composition, where V is the growth tip velocity and m is a factor ranging from 1/3 to 1/2.

Hansen, Hellawell *et al.*[19] developed a six-step physical model in order to explain equiaxed crystal formation, and consequently, columnar-to-equiaxed transition (CET). The model considered remelting as a source for the equiaxed grains and the thermosolutal convection an essential transport mechanism in the mushy zone and in the open bulk. The model was compared with experimental investigations on the transparent system NH_4Cl-H_2O. Observations demonstrate that ripening and fragmentation by remelting take place constantly and depend on the permeability of the mush, which varies along its depth.

In previous works,[20–22] the authors have presented in detail the flow behavior and characteristics during a mainly columnar solidification of an NH_4Cl alloy in a thin (1 cm thickness) cast cell at liquid height of 8 cm. However, few equiaxed crystals occurred during the turbulent flow regime, in the region closed to the lateral mushy zone. This paper verifies the hypothesis that a higher liquid height in the cast cell (thus stronger buoyant melt flow) will enhance the columnar-to-equiaxed transition (CET).

II. EXPERIMENTAL PROCEDURE

For the experiments undertaken for this paper, a cell of 3 cm thick and 10 cm width was chosen and the height of the liquid in the cell was 9.5 cm. With this height we expect to increase the Rayleigh number, which should result in a stronger buoyant flow. The concentration of the ammonium chloride for the NH_4Cl-H_2O solution was varied between 27 and 31 wt pct. The solution was prepared as follows: the respective amount of NH_4Cl was weighted then distillate water was added to obtain the respective concentration. The above mixture was heated up while stirring until 315.15 K (or 318.15 K). In the meantime, the cast cell's walls were heated until 315.15 K (or 318.15 K) by use of a bath.

When the desired temperature was reached, the liquid solution was poured into the cell and left idle for approximately 15 minutes. After this time the thermal bath was set to 278.15 K, thus the cooling started. In order to measure the temperature evolution in time, several thermocouples were inserted in the cell's wall and one thermocouple in the bulk in the middle of the cell. During the solidification experiment with ammonium chloride, a thermocouple inserted into the bulk melt would have disturbed the solidification. Thus thermal measurements of the bulk temperature evolution were performed using pure water. The cooling was found to be uniform for the three walls, only a minute temperature difference of smaller than 0.1 K was recorded between them. The temperature difference between the middle of the bulk and the wall is reported in Figure 1 for the cases of 9.5 cm liquid height and 8 cm liquid height, respectively. The cooling rate applied by the thermal bath was the same in the two cases.

During the solidification process, pictures were taken simultaneously with two CCD cameras. One camera (green filter) was used to catch the ammonium chloride solid growth and the other camera (orange filter) to follow the liquid melt, *via* the Rhodamine-coated polyamide seeding particles. The images were recorded using the commercial software *Dynamic Studio*, generally every minute one set of 10 images. The time between each image in one set is 250 ms. The data treatment (PIV correlations) was also processed with the *Dynamic Studio* software. More details on the PIV technique can be found in previous works.[20–22] Once the velocities are extracted, the flow kinetic energy (KE) can be calculated as follows:

$$\mathrm{KE} = \sum_{\mathrm{IA}} \frac{1}{2} U^2 \times \mathrm{Vol} \times \rho / \mathrm{IA}, \qquad [1]$$

where IA is the total number of PIV interrogation areas (in the mushy zone the velocity vectors are zero), Vol is the volume occupied by the liquid in the cell, and $\rho = 1078$ is the liquid ammonium chloride density.

III. RESULTS

A. *The Problematic*

For the sake of providing greater clarity, the present section aims to illustrate the topic of the present publication with a single comparison. More results and a deeper analysis follow in the next sections.

1. *Flow kinetic energy*

Figure 2 presents two plots of the flow kinetic energy extracted, one during a equiaxed solidification experiment (red curve) and second during a columnar solidification experiment (black curve).

2. *Flow regimes during solidification*

A detailed description of the different flow regimes encountered during columnar solidification of ammonium chloride can be found in previous papers.[20,22] However, to gain a better understanding, a short overview of flow regimes found in currents experiments is in Figure 3. The flow vector maps corresponding to these regimes for a typical equiaxed experiment (shown in Figure 2, red curve), performed at 29.6 wt pct NH_4Cl in the 3-cm-thick cell at a liquid height of 9.5 cm, are presented: (a) thermal symmetric (TH) flow regime, when only the thermal convection plays a role; (b) turbulent solutal flow (TU) regime; (c) equiaxed-driven flow (EQ) regime when a lot of equiaxed occurred (this flow regime does not exist during experiment with mainly columnar solidification); and (d) a meandering flow (MF) regime when the double diffusion becomes the main event. Generally the flow regimes are the same as in the columnar solidification, the only major difference is the presence of the equiaxed-driven flow regime characterized by the intense sedimentation of equiaxed crystals. The melt flow during this regime is laminar due to the laminarization triggered by the

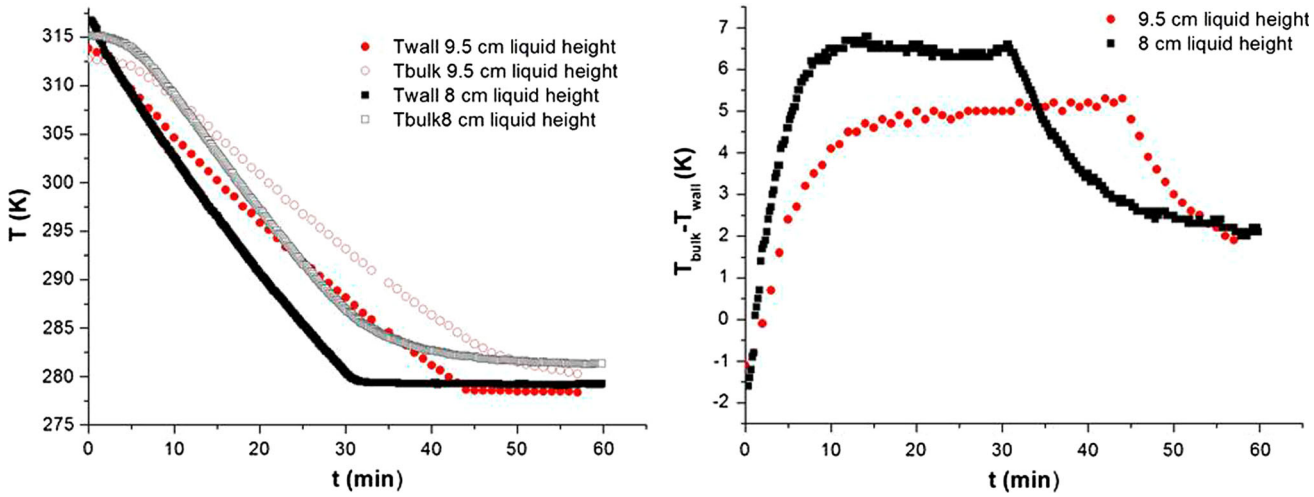

Fig. 1—Temperature evolution in the 3-cm-thick cell at 8 cm (lower cell) and 9.5 cm (higher cell) liquid height.

higher effective viscosity of the liquid-equiaxed mixture. This phenomenon of laminarization was locally observed in regions of high equiaxed crystal density, meanwhile the bulk liquid remained turbulent.[21]

3. *Relationships between flow kinetic energy and equiaxed crystals occurrence*

By relating the graph of Figure 2 with the observations of Figure 3, a correlation between the flow kinetic energy (KE) and the occurrence or not of the equiaxed crystals can be clearly asserted. The present paper aims to answer the following questions: (1) From the heterogeneous nucleation and fragmentation which can explain the best of the equiaxed occurrence? (2) How is the equiaxed crystal occurrence and the flow hydrodynamics related? (3) Is one or two way coupling?

The following presents the results of additional experiments with the 9.5 cm high cell. The average melt velocity and the solid front velocity will be extracted from the experimental data and the relationship between the two will be investigated. The experiments are divided into two series: a lower ammonium chloride concentration group with 27, 27.58, and 28 wt pct NH_4Cl and the higher concentration group with 29.6 and 31 wt pct NH_4Cl. The analysis focuses on the results from the nucleation and fragmentation perspective, and on their relationship with the melt flow magnitude.

B. *Lower Concentration Group*

1. *Flow and solidification stages*

For the lower concentration group (27, 27.58, and 28 wt pct), solidification started around 25 minutes after cooling from 315.15 K was initiated. The solid appeared along the lateral walls first, under small islands, which developed further until they completely covered the 3 cell's walls (side and bottom walls). At 32, 33, and respectively 38 minutes, equiaxed crystal formation occurred next to the lateral mushy zone. Shortly after, 2 to 3 chimneys emerged from the bottom mush. A large number of equiaxed crystals appeared around these

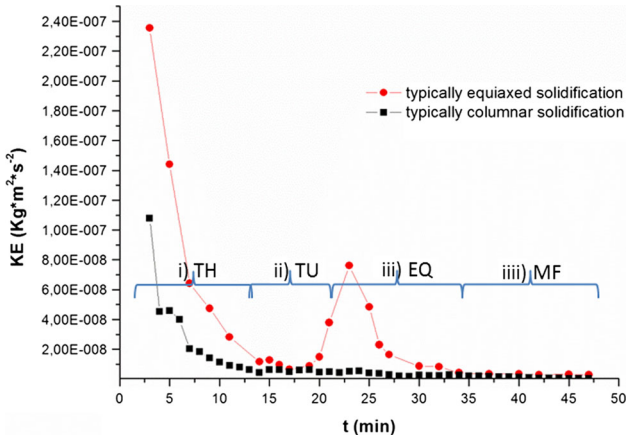

Fig. 2—Flow kinetic energy extracted during a typical equiaxed (9.5 cm high) and a typical columnar (8 cm high) solidification experiment. The time extension of the different flow regimes for the typically equiaxed solidification experiment: (TH) thermal buoyancy, (TU) turbulent-plume flow regime, (EQ) equiaxed-driven flow, (MF) meandering flow regime (Color figure online).

chimneys. After 45, 54, and 50 minutes, respectively, from the inception of cooling, the manifestation of equiaxed crystals stopped, but solidification continued in the form of columnar dendrites. Generally, the equiaxed event lasted about 13 minutes (21 minutes for the 27.58 wt pct experiment, red on Figures 4 and 5).

2. *Mush growth*

The mushy zone growth during the solidification process, was extracted from the pictures. We then estimated the 2D surface occupied by the mushy region; the percentage is named "percentage of apparent mush" in the cell. These results are plotted in Figure 4, where it is evident that the final amount (in pct) of apparent mush is situated around 52 to 55 pct of the cell, except for one experiment (black 28 wt pct on Figure 4) where the final mush is much greater, 71 pct.

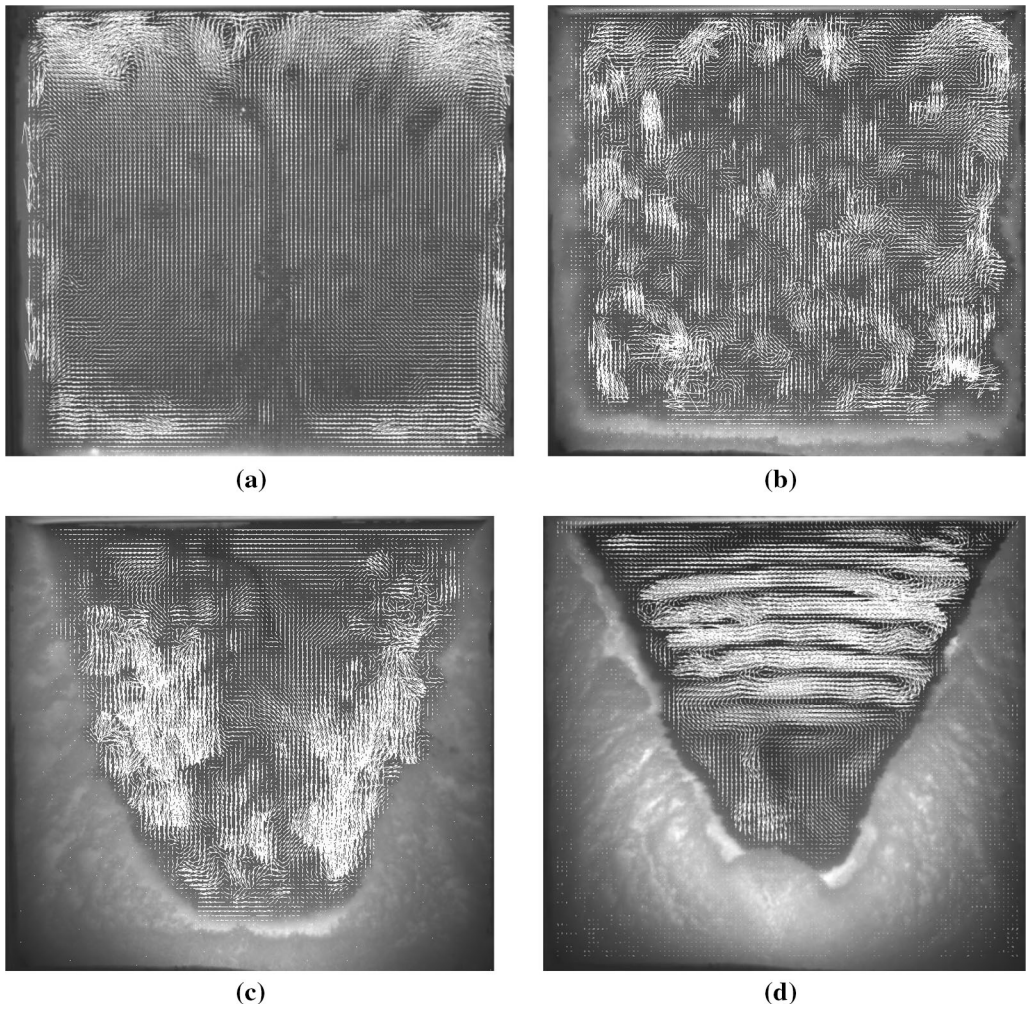

Fig. 3—Flow vector maps at different times corresponding to different flow regimes during the equiaxed solidification of 29.6 wt pct NH_4Cl performed in the 3-cm-thick cell at a liquid height of 9.5 cm: (*a*) Thermal Buoyancy (TU) at 14 min; (*b*) Solutal turbulence (TU) at 20 min; (*c*) Equiaxed-driven flows (EQ) at 25 min. with a lot of equiaxed crystals; (*d*) Meandering flow (MF) at 45 min.

3. *Flow kinetic energy*

The evolution of the liquid phase KE over time was calculated (Eq. [1]) using the measured velocity magnitude U, obtained by adaptive PIV correlation, applied on the pictures where only liquid phase velocity was measured (not the equiaxed grains). The results for 27, 27.58, and 28 wt pct ammonium chloride respectively are displayed in Figure 5. The KE values calculated with Eq. [1] are actually an average flow KE over the volume of the cell.

Although experiments started under identical initial conditions, we could expect the magnitude of the flow KE at the very beginning to be equal for all experiments. The system seems to be very sensitive to minor temperature variation and the initial flow KE values were found to be different between all of the cases. Generally, at the beginning of the cooling process, the flow is at its most powerful, driven by thermal buoyancy. Along the vertical walls, the strong, descending jets are difficult to resolve with the present PIV system, thus these velocities are missing in the calculation of the flow KE. The error

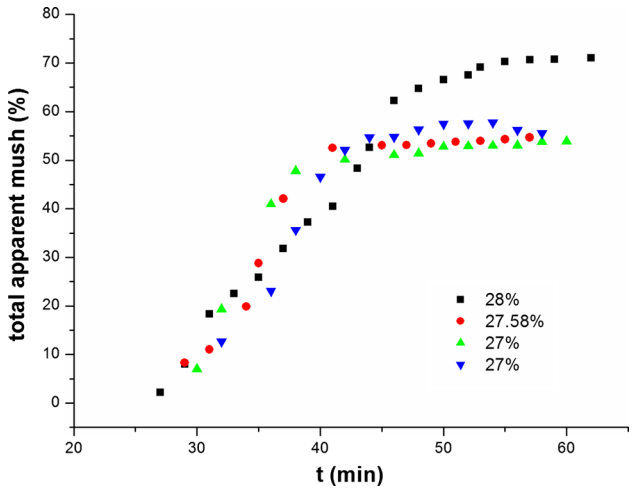

Fig. 4—Percentages of apparent mush in the cell during the solidification of 27 to 28 wt pct NH_4Cl alloys.

concerns only the first minutes when the jets are very thin. Later these jets thicken and then disappear especially once the solidification begins.

The decreasing trend is the same (except green curve on Figure 5). Before solidification occurs, only thermal buoyancy is present and as the temperature difference diminishes, the flow KE decreases. Despite the different hydrodynamic history after 15 minutes, the flow KE finally reaches a similar magnitude for all experiments.

Once the onset of equiaxed crystals begins (around 33 and 37 minutes, see Table I), an increase in the flow KE is clearly apparent (Figure 5). During the equiaxed grain event, 2 to 3 chimneys could be observed. A peak in the flow KE takes place after the commencement of the equiaxed crystal event. This peak can be correlated to the time when a maximum of equiaxed grain is created. The peak values are considerable and in the same order of magnitude for all experiments.

The equiaxed crystal rain was extinguished 45 to 54 minutes after cooling started. Later, only individual grains appeared locally intermittently. After the extinguishing, the flow KE falls down to minimal magnitude values, similarly to what was measured during purely columnar solidification experiments.[20]

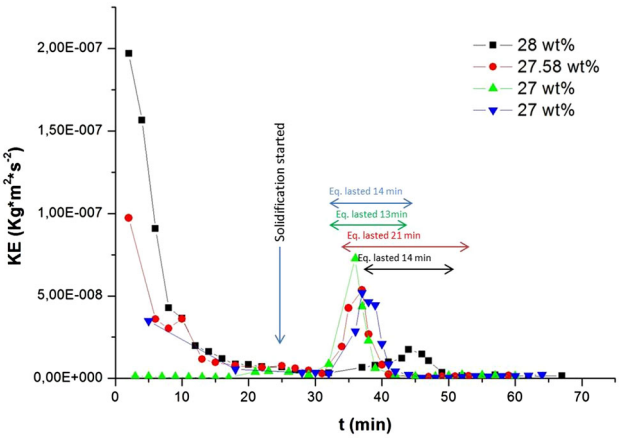

Fig. 5—Flow kinetic energy (KE) during the solidification of 27 to 28 wt pct NH_4Cl alloys ("Eq. lasted" stands for Equiaxed lasted for) (Color figure online).

C. *Higher Concentration Group*

1. *Flow and solidification stages*

For the higher concentration group (29.6 and 31 wt pct) study, the flow behavior, consequently the flow KE evolution, are similar to the example previously described for the lower concentration group. However, during the generation of equiaxed grains, no chimney phenomenon occurred. Therefore, the equiaxed rain event was much steadier and calmer compared to the low concentration group, where the chimneys produced equiaxed crystals in a far more chaotic and distorted manner. In Table I the times when the most important phenomena were visible during solidification (solidification start and equiaxed crystal occurrence) are documented for all series of experiments (low and high concentrations).

The cooling was initiated from 315.15 K (for the 29.6 wt pct experiment) and 318.15 K (for the 31 wt pct experiments), and solidification occurred at 14 minutes (29.6 wt pct), 9 and 6 minutes (31 wt pct) afterwards, respectively. At 17 minutes (29.6 wt pct), 10 and 8 minutes (31 wt pct) after the onset of the cooling, respectively, equiaxed crystals started to occur. The equiaxed grains were distributed throughout the bulk melt and their number was important.

2. *Mush growth*

The evolution of the apparent mush percentage was estimated and the final values reached 55 pct (29.6 wt pct), 66 pct, and 73 pct (31 wt pct) (Figure 6).

3. *Flow kinetic energy*

The evolution of the flow KE (Figure 7) follows the same decreasing tendency until the occurrence of the first equiaxed crystals at 17 minutes (29.6 wt pct), 10 and 8 minutes (31 wt pct). Beginning with these times, an increase in the flow KE can be observed and a peak was witnessed several minutes afterwards. This applies less to the green curve (31 wt pct) on Figure 7. For the 29.6 wt pct experiment (black curve on Figure 7) a clear peak can be observed at 23 minutes. This peak followed the occurrence of a large amount of equiaxed crystals at 19 minutes. However, the maximum of equiaxed crystals was achieved around 25 minutes. At this time the flow

Table I. Times When Most Important Phenomena (Start of Solidification, Equiaxed Crystals) Occurred During Solidification Experiments

NH_4Cl Concentration	Initial T of the Bath When Cooling Started (t_0)	T_{wall} When Cooling Started	t_{solid} (Time When Solid Occurred After t_0)	Time When Flow KE Peak Occurred	Equiaxed Crystals (Start)	Equiaxed Crystals (Maximum)	Equiaxed Crystals (End)
28 wt pct	315.15 K	313.05 K	25 min	44 min	37 min	44 min	51 min
27.58 wt pct	315.15 K	313.95 K	25 min	37 min	33 min	38 min	54 min
27 wt pct	308 K	306.55 K	25 min	36 min	32 min	36 min	45 min
27 wt pct	315.15 K	313.35 K	28 min	37 min	32 min	40 min	46 min
29.6 wt pct	315.15 K (42 °C)	315.35 K (42.2 °C)	14 min	23 min	17 min	25 min	46 min
31 wt pct	318.15 K (45 °C)	315.75 K (42.6 °C)	9 min	19 min 27 min	10 min	19 min 26 min	37 min
31 wt pct	318.15 K (45 °C)	315.35 K (42.2 °C)	6 min	16 min 24 min	8 min	12 min	32 min

kinetic energy started to decrease. For the green experiment (31 wt pct) in Figure 7 the very first equiaxed grains occurred 8 minutes after the cooling started and the event took place for 24 minutes. The increase in the flow KE is lower, and practically no peak can be observed. However, the maximum value was reached at 16 minutes and the maximum of equiaxed crystal was at 12 minutes. For the other experiment at 31 wt pct (red curve on Figure 7) two peaks are visible and each can be linked with an equiaxed event. The first peak at 19 minutes takes place simultaneously with many equiaxed grains. The second peak at 27 minutes follows the occurrence of a large amount of equiaxed crystals at 26 minutes. In this case, the equiaxed crystals lasted for 27 minutes.

Here again, as in the lower concentration group, a clear correlation was evident between the onset of the equiaxed crystals and the flow magnitude and behavior. In the flow kinetic energy evolution over time, an increase is immediately observed after the equiaxed crystals are produced and a peak takes place simultaneously (31 wt pct red) or very short before (29.6 wt pct black) or after (31 wt pct green) the maximum amount of equiaxed grains is reached.

In Figure 8 the total flow kinetic energies for all experiments performed in the thick cell at 9.5 cm liquid height are reported but all the times were set to zero at the start of solidification. It is remarkable that all the KE peaks superpose except for the 28 wt pct experiment (dark blue curve). Very important to notice is that the peaks occur at a certain time after the solidification started and this time seems to be the same for almost all experiments. The maximum values are all in the same order of magnitude 2 to 8 $\times$ 10^{-8} kg m^{-2} s^{-2}.

D. *Average Melt Velocity Related to Solid Front Growth*

From the calculated flow kinetic energy (KE), we extracted the average flow velocity using the following relation $\overline{U} = \sqrt{2\mathrm{KE}/\mathrm{Vol} \times \rho}$, where Vol represents the volume occupied by the liquid melt and ρ is the ammonium chloride density. Using the PIV pictures as those presented in Figure 3, the average solid bottom front velocity was also extracted: $V_{\mathrm{front}} = (\mathrm{d}S/\mathrm{d}t)/L$, where S is the apparent surface occupied by the mush and L is the length of the solidification front.

Figure 9 presents the velocity growth of the bottom solid front *vs* the average melt flow velocity. Generally, at small front velocity values correspond small average flow velocities and at large front velocities are associated with high melt velocity values. The kaki points represent the values where equiaxed crystals are not present (late time in solidification). At small velocity growth (0.2 mm s^{-1}), generally no equiaxed crystals are present. Nevertheless, some values corresponding to equiaxed crystal occurrence are present in this corner of small solid front velocity growth and small average flow velocity. In these cases, even if the average flow velocity is low, it does not mean that it will be low everywhere. Locally, high velocities can exist with the presence of equiaxed crystals.

Figure 9 illustrates the fact that the intense melt flows are more likely associated with the presence of equiaxed crystals. This goes in the direction that large flow velocities enhance the occurrence of equiaxed crystals, but the reciprocal might also be true. In the Discussion chapter the flow melt influence will be analyzed and a mechanism will be proposed for the equiaxed crystal creation.

IV. DISCUSSION AND ANALYSIS

In this chapter the analysis will cover the following steps: first the comparison between a mainly columnar and mainly equiaxed experiment, second the analysis of nucleation and fragmentation as origin for the equiaxed grains, and last the mechanism proposed to explain the CET and the important role played by the melt flow.

A. *Comparison Between a Typically Columnar and Equiaxed Solidification Experiments*

In Figure 10, the flow kinetic energy for a mainly columnar experiment, performed in the 3-cm-thick cell

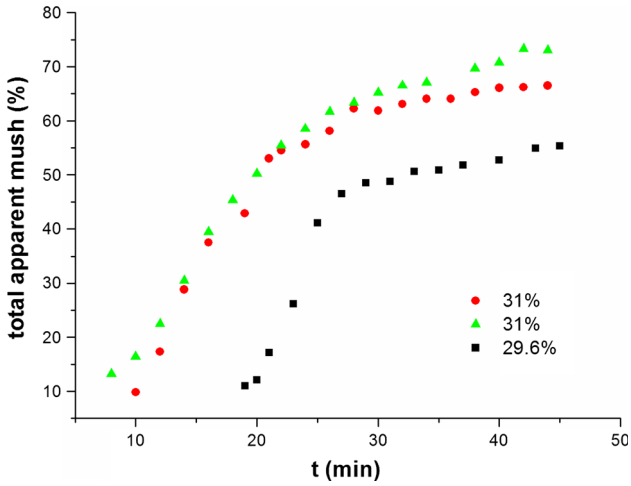

Fig. 6—Percentages of apparent mush in the cell during solidification of 29.6 and 31 wt pct NH_4Cl alloys.

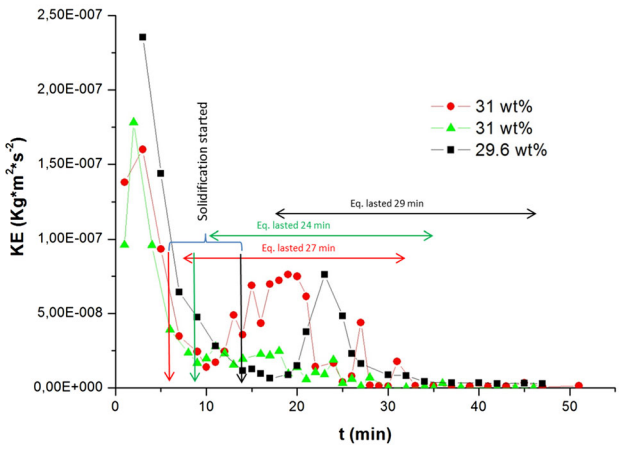

Fig. 7—Flow kinetic energy (KE) during solidification of 29.6 and 31 wt pct NH_4Cl alloys (Color figure online).

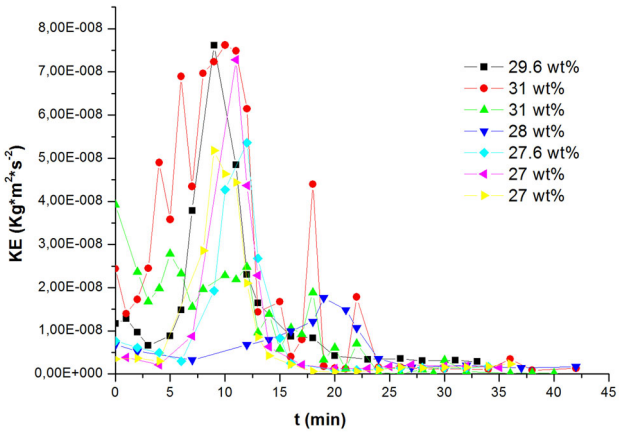

Fig. 8—Comparison of flow KE starting from the time when solidification occurred in the 9.5 cm high cell during the solidification of different ammonium chloride concentrations from 27 to 31 wt pct (Color figure online).

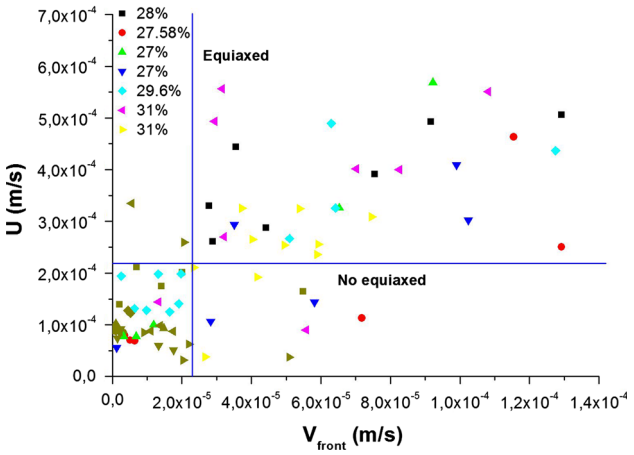

Fig. 9—Average velocity flow *vs* velocity front for different NH_4Cl alloy concentrations during solidification at 9.5 cm liquid height. Colored points stand for presence of equiaxed. The kaki points report situations when no equiaxed crystals occurred anymore (Color figure online).

at 8 cm liquid height (lower cell), is compared with flow KE for a mainly equiaxed experiment, performed in the present investigation with a 9.5 cm height cell. The ammonium chloride concentration used in the two cases is strictly the same (29.6 wt pct). The starting wall's temperature for both experiments was fixed at 315.15 K at the thermal bath, and the cooling rate was homogeneous (Figure 1).

The flow KE starting values are lower for the mainly columnar experiment (8 cm liquid height) than for the equiaxed experiment (9.5 cm liquid height) but in the same order of magnitude. This can be explained by the difference in the Rayleigh number. It is very clear that the global trend of the flow kinetic energy evolution with time (Figure 10), which expresses the flow behavior, is dramatically different in the case of a columnar solidification experiment, compared with an equiaxed solidification experiment. In the case of the mainly columnar experiment, the flow kinetic energy decreases

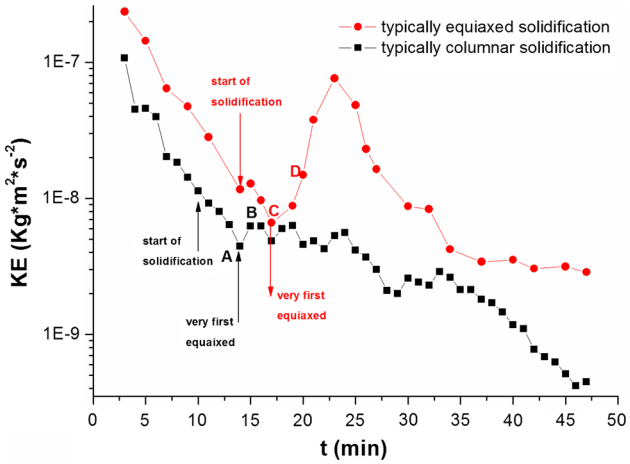

Fig. 10—Flow KE comparison at 8 cm liquid height (mainly columnar solidification) and 9.5 cm liquid height cell (equiaxed solidification) in logarithmic scale (Color figure online).

continuously and exponentially, and the values are usually smaller than in the case of the mainly equiaxed solidification experiment.

For the equiaxed solidification case (9.5 cm liquid height), the flow kinetic energy decreases until the start of equiaxed crystal apparition and then a significant increase in the flow kinetic energy takes place. In Figure 10, note that in the typical columnar solidification (black curve), the flow KE decreases continuously until the point A. The point A (14 minutes after cooling was started) marks the beginning of a very small increase in the flow KE and corresponds to the time when the solutal natural convection starts to become significant. This increase continues until point B, but then the flow KE decreases back with some oscillations. These small KE oscillations are believed to be induced by the solutal buoyancy, which creates a turbulent non-coherent flow regime.

The flow velocity map corresponding to point B (Figure 10) is shown in Figure 11(a). This flow doesn't have a stable structure neither in time nor space (Figure 11(a)). The flow will rise at some points and then come down following a sinusoidal wave from right to left (Figure 11(a)). The magnitudes of the flow in the bulk area are tiny (0.01 mm s^{-1}) with some maxima of 0.3 to 0.5 mm s^{-1} in the green areas. In the mush the flow cannot be visualized, it can only be observed where it enters the mush and where it comes out. At the right bottom corner (Figure 11(a)) the flow falls down with high velocity and immediately near it goes up (follow the big white arrow Figure 11(a)). In this same area only few equiaxed crystals were noticed.

Concerning the mainly equiaxed solidification experiment (red curve on Figure 10), the situation is completely different. At point C the very first equiaxed crystals were present and immediately the flow KE increases. The increase from point C to point D is similar to the increase observed for the black curve from point A to B, the only difference is that the corresponding flow is stronger at point C than at point A.

Moreover, for the mainly equiaxed solidification the increase continues after the point D and the occurrence of equiaxed crystals is massive. The magnitude of the flow at point D (see flow velocity map on Figure 11(b)) indeed shows maximum values are larger than at point B (see flow velocity map on Figure 11(a)) and these maximum values are spread all over the length of the mushy zone. Of course the flow in the mush is not visible, but one can assume that if the flow is high in the vicinity on the mush, it enters the mushy zone and can transport many dendrite fragments. The bulk is particularly patterned, presenting many areas with relatively large velocity ~ 0.6 mm s^{-1} (green zones on Figure 11(b)). The flow is strong and its impact is marked on the temperature and concentration distribution, creating local undercooled zones even far in the bulk and thus the possibility of equiaxed dendrite growth. In Figure 11(b), the zone delimitated by the red oval already contains many equiaxed crystals distributed everywhere (evident in Figure 11(c)). The flow present at point D is strong enough to have carried out many dendrite fragments and these fragments will have grown into equiaxed fragments in the bulk.

When equiaxed crystals form in the bulk, they grow and then fall down and accelerate the melt flow with their fall. This can be seen in Figure 11(b) inside the region delimitated by the red oval, the flow is downward in many places, which is the mark of falling equiaxed

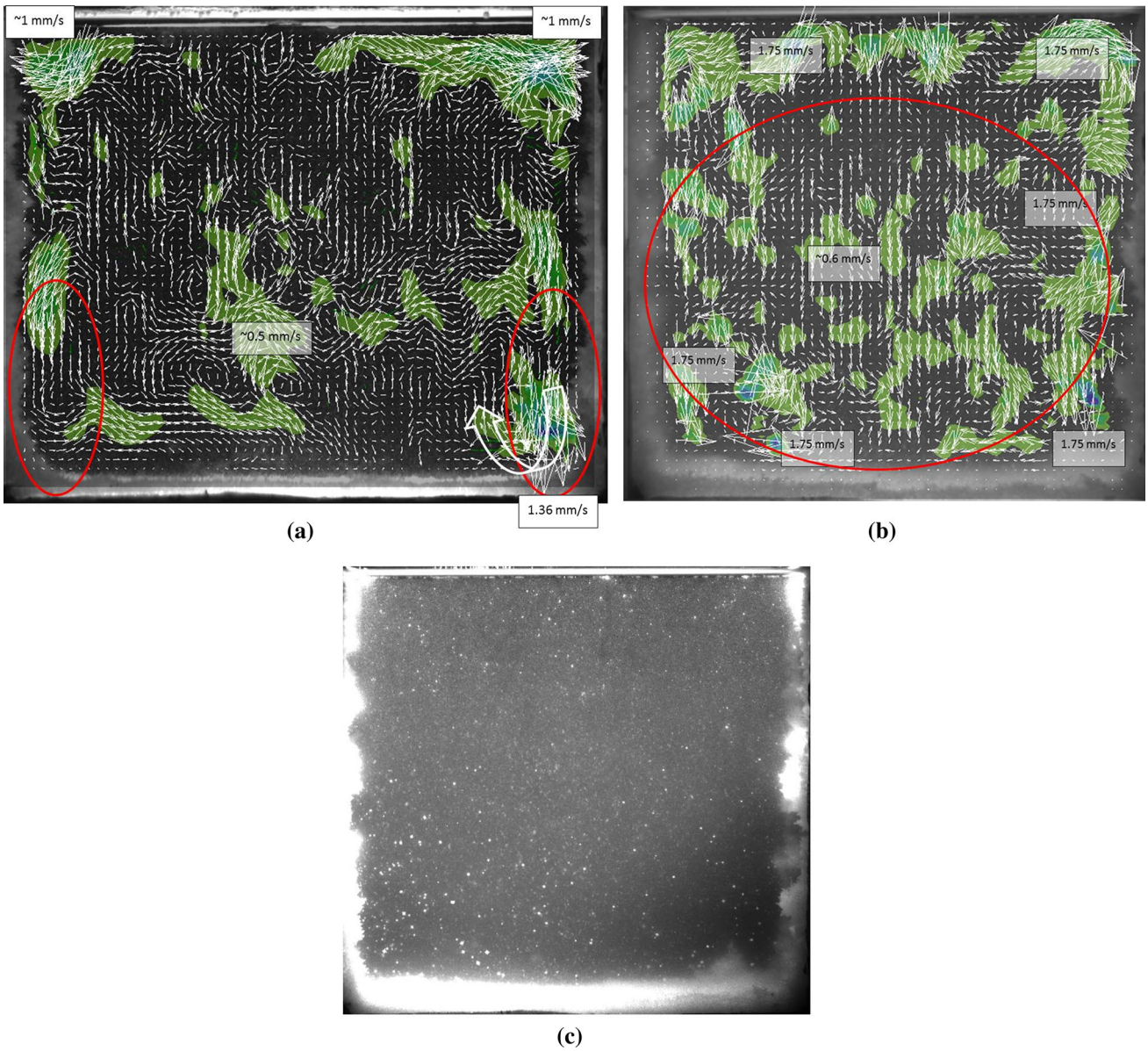

Fig. 11—(*a*) Flow velocity map at 16 min (point B on Fig. 10) after cooling started during the mainly columnar solidification experiment (maximum flow velocity values at top corners ~ 1 mm s^{-1} and right bottom corner ~ 1.36 mm s^{-1} and equiaxed crystals only present next to the lateral mush inside the 2 red ovals left and right); (*b*) Flow velocity map at 20 min (point D on Fig. 10) after cooling started during the mainly equiaxed solidification (large velocity values all along the length of the mushy zone and at the top ~ 1.75 mm s^{-1} and equiaxed grains are present everywhere in the zone delimited by the red oval); (*c*) Equiaxed crystals in the bulk at the same time as the flow map shown in Fig. 11(b)) (Color figure online).

crystals driving the flow. The melt flow will thus penetrate the bottom or lateral mushy zone. When leaving the mushy zone, this flow will bring into the bulk liquid a certain number of dendrite fragments. These fragments arriving in the undercooled melt will eventually grow and drag the flow in their fall. This phenomenon can sustain and intensify itself as long as the concentration and temperature in the bulk are adequate to enable the dendrite fragments to grow into equiaxed crystals.

An evaluation of the peak height in the flow KE time evolution was performed. The ratio between the maximum peak value and the base value (before the increase of the flow KE) was calculated (as shown in Figure 12(a)). These ratios were compared and a net tendency arises: In the case of mainly columnar experiments (data taken in Reference 20) the ratio situates in-between 1 and 2, for the present experiments with strong presence of equiaxed crystals the values set from 11 to 33. For the example showed in Figure 12(a) the ratio is equal to 11.51. Figure 12(b) presents the picture of the equiaxed crystals and mush at 2 minutes after the peak. Many equiaxed crystals are visible, they seem to come out from the lateral mush and fall down at the corners. Figure 12(b) can be correlated to Figure 12(c) where the flow map velocity is shown for the same time (2 minutes after the peak) and consequently it can be imagined that the flow comes out from the lateral mushy zone (drawn big arrows) where the equiaxed crystals occurred but also re-enter the mush where equiaxed crystals descend.

Comparing the percentage of the cell filled with mush over time, clear differences can be witnessed between a typically columnar and a typically equiaxed solidification experiment (Figure 13(a)). The solidification started at 10 minutes in the 8 cm liquid height cell, and at 14 minutes in the 9.5 cm liquid height cell (temperature gradient in the 9.5 cm cell is lower than in the 8 cm cell (Figure 1), thus the time to reach the solidification temperature was longer. However, until 23 minutes, the solid front growth is equivalent for the two cases (typically columnar and typically equiaxed). At 21 minutes an acceleration of the solidification front speed can be observed for the equiaxed case (Figure 13(a), red curve). This acceleration is related to the equiaxed event which started already at around $t = 17$ minutes after the cooling started, but the maximum strength was reached at $t = 25$ minutes. By the end of the solidification process (~ 1 hours after the cooling started) the final amount of apparent mush is 5 pct larger in the case of the experiment with equiaxed crystals than in the columnar case. This can be explained by the fact that columnar mush has a regular structure, with lower permeability. In opposite, the occurrence of equiaxed crystals in front of the columnar zone increases the permeability and consequently the volume occupied is larger. The final shape of the mushy zone is also different for the two cases (Figures 13(b) and (c)). For the typically columnar case the final shape is fine and regular with a flat bottom mush. For the typically equiaxed case, the final shape of the mush is irregular, forming a V profile. Such differences in shape and growth speed have been verified for all present and past experiments.[20–22]

B. *Interpretation Based on the Assumption that Equiaxed Crystals are Created by Nucleation*

The heterogeneous nucleation implies the existence of a substrate (mold or foreign particles), which can be simply impurities or refining particles. Oldfield[23] has demonstrated experimentally that the grain's density N is related with the maximum undercooling (attained at recalescence):

$$N \propto A\Delta T_u^2 \qquad [2]$$

In this case nucleation is instantaneous and the nucleation sites have different activation potentials at characteristic temperatures. The size distribution of the foreign particles is essential in the activation of nucleation as the undercooling increases.

Once the creation of the first nuclei has taken place, the second growth phase can commence. As the nucleation increases, the growth rate, V will also rise, since the nucleation will provide sites on which to grow. As ΔT_u increases, the growth rate V will approach that of uniform growth, $V \sim$ const. ΔT_u, as the nuclei already created provide sufficient spots to grow.

In addition, to grow nuclei it need to spend time in the undercooled region. Hence larger is the undercooled zone better are the conditions for growth.

Based on the above consideration, Hunt[24] proposed a model for the transition from columnar to equiaxed growth. Two characteristic length can be considered: first the undercooled length in front of the columnar zone, $L_C = \Delta T_C/G$ and second the space between the nuclei forming the equiaxed zone, L_N. The latter is related to the density of nuclei, $L_N = N^{-1/3}$. Remark that larger N permits the equiaxed zone to grow more rapidly and larger ΔT_C increases the columnar front undercooling and thus the length over which the equiaxed grains can grow. It can be resumed that the equiaxed zone is favored at low temperature gradient and/or high undercooling. A correlation between the columnar front growth and the equiaxed crystal occurrence is also considered in this model and the relation is shown in Eq. [3]:

$$V = A \cdot T_C^2, \qquad [3]$$

where A is a factor which cumulates the solute rejection at the dendrite tip. It is shown that the undercooling is connected with the columnar velocity front, higher undercooling corresponds to larger growth velocity.

During current solidification experiments the temperatures were measured for the 8 cm liquid height case and 9.5 cm liquid height case (Figure 1). The temperature difference between the bulk and the wall is larger in the case of 8 cm liquid height, thus the temperature gradient is higher in this case. With the following equation:

$$L_C = \frac{\Delta T_C}{G} = \frac{\Delta T_C * \Delta x}{\Delta T}, \qquad [4]$$

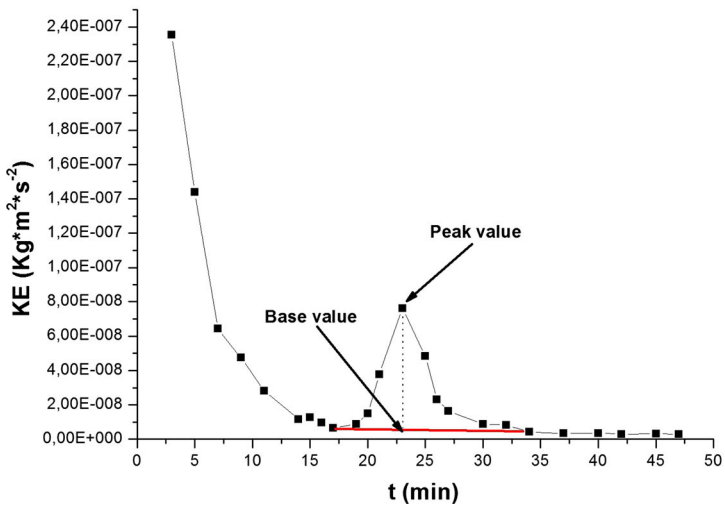

(a)

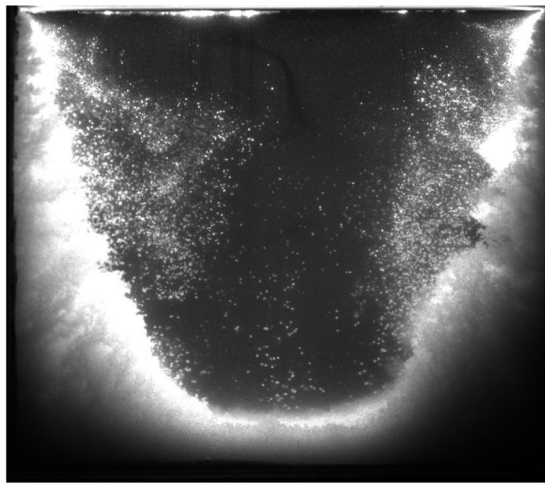

(b)

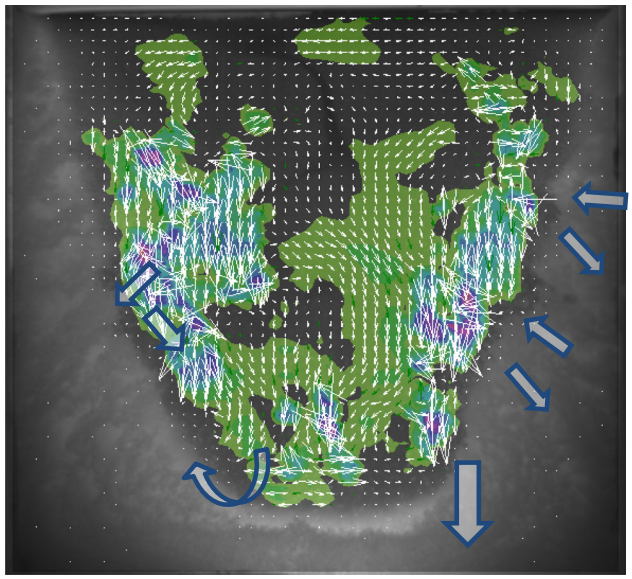

(c)

Fig. 12—(*a*) Schema of the baseline value and peak value in the case of equiaxed solidification; (*b*) Picture of experiment with mushy zone and equiaxed crystals fall at about 2 min after the peak; (*c*) Liquid phase flow velocity map at 2 min after the peak. Large vectors represent the probable direction of the liquid flow out or into the mushy region. These vectors are emanating from the mushy zone in areas where equiaxed crystals suddenly appeared and re-entering the mushy zone where equiaxed crystals fall down.

the length of the undercooled region δ can be estimated for a given global temperature gradient $G \cong \frac{\Delta T}{\Delta x}$ (where $\Delta T = T_{\text{bulk}} - T_{\text{wall}}, \Delta x$ is the distance between the wall and the middle of the bulk) and a certain undercooling $\Delta T_C = T_l - T_C$, (where T_l is the liquidus temperature corresponding to the initial alloy concentration, and T_C is the temperature of the columnar front). In the case of the 8 cm liquid height, the undercooled region's length is smaller than for the 9.5 cm liquid height case. Due to the greater length of the undercooled region in the higher cell, the chances of obtaining a nucleation of equiaxed crystals are larger than in the lower cell.

Introducing relations given in Eqs. [4] into [3], the front velocity growth can be correlated with the length of the undercooled region, $V \propto L_C^2$. In Figure 9 it can be observed that for front velocity larger than 3 μm s^{-1}, hence large undercooled zone, equiaxed crystals occurred (colored points). For lower columnar front growth velocity, thus small undercooled zone, no equiaxed crystals happen (kaki points). These observations support relations from Eqs. [3] and [4]. On the other hand, the kaki points (when no equiaxed occurred) are located late after the cooling has started, when thermal and solutal forces diminish. Equiaxed crystals (colored points on Figure 9) occur when the themosolutal forces are intense. Considering only the nucleation theory, no clear correlation can be made between the flow strength and the equiaxed crystal creation, because the flow exerts no direct influence on nucleation. However, the correlation between high V

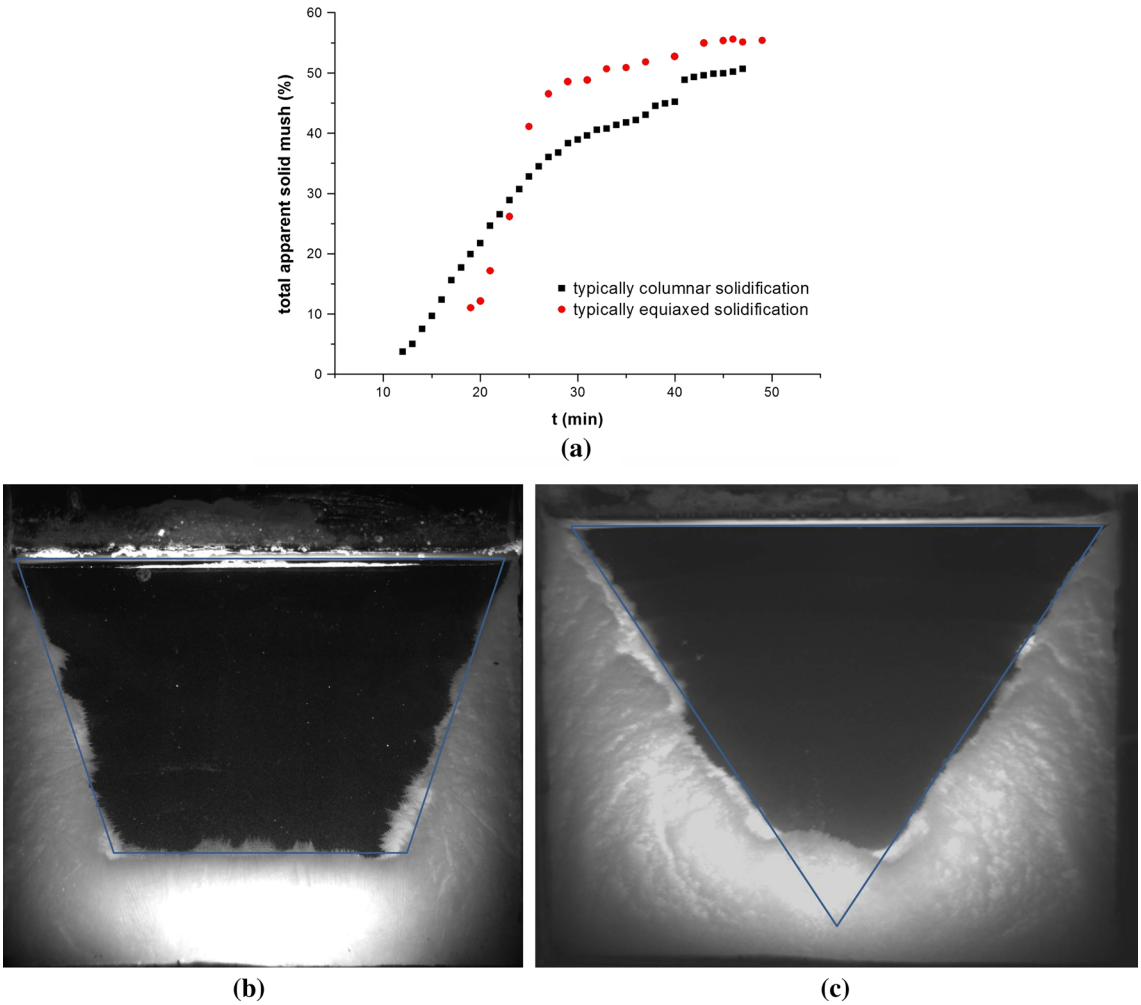

Fig. 13—(*a*) Evolution of the percentage of apparent mush in the cell in the 8 and 9.5 cm height cell during the solidification of 29.6 wt pct ammonium chloride; (*b*) Final shape of the mush in the 8 cm height cell, typical columnar solidification; (*c*) Final shape of the mush in the 9.5 cm height cell, typical equiaxed solidification (Color figure online).

and large melt flow velocity can be understood by the enhancement of solutal buoyancy when the front velocity increases, as lighter solute is rejected at the solidification front. In addition, the falling equiaxed crystals drive the flow due to drag interaction and will result in flow acceleration. It has been seen in experimental investigations that in areas with a large number of equiaxed crystals, high melt flow velocities are generated. In summary, there is a one-way coupling: nucleation rate can directly influence the flow, but the flow cannot directly influence the nucleation rate. In next section, a much stronger coupling will be shown if we assume equiaxed crystal growth from fragments expelling from mushy zone.

C. *Interpretation of the Results Based on the Fragmentation Phenomena*

Ideally, in order to estimate the potential strength of equiaxed creation by fragmentation, it is necessary to quantify the number of fragments leaving the mushy zone. Inside the mushy zone, the number of available dendrite fragments is directly correlated to the number density of primary, secondary, and tertiary arms. These arms are mainly controlled by the temperature gradient G and the front velocity V.

Two theories were developed by Hunt,[24] Kurz, and Fisher,[25] who proposed a power law correlating the primary λ_1 arm spacing and the columnar front velocity V, the gradient G, and the initial alloy concentration C_0. In the two models, only the constant K is different and the respective relation is shown in Eq. [5]:

$$\lambda_1 = KC_0^{0.25}G^{-0.5}V^{-0.25} \qquad [5]$$

where K is connected with: the Gibbs–Thomson coefficient, the liquidus line slope, the solute partition coefficient, and D the liquid solute diffusivity.

Considering this relation, we can conclude that the larger the velocity growth, smaller the dendrite arm spacing λ_1 and λ_2, thus more branching occurs.

Experimental observations on Succinonitrile (SCN)–carbon tetrabromide (CTB) alloy solidification[26] have been made for different CTB concentrations, constant temperature gradient (7.5 K mm^{-1}), and

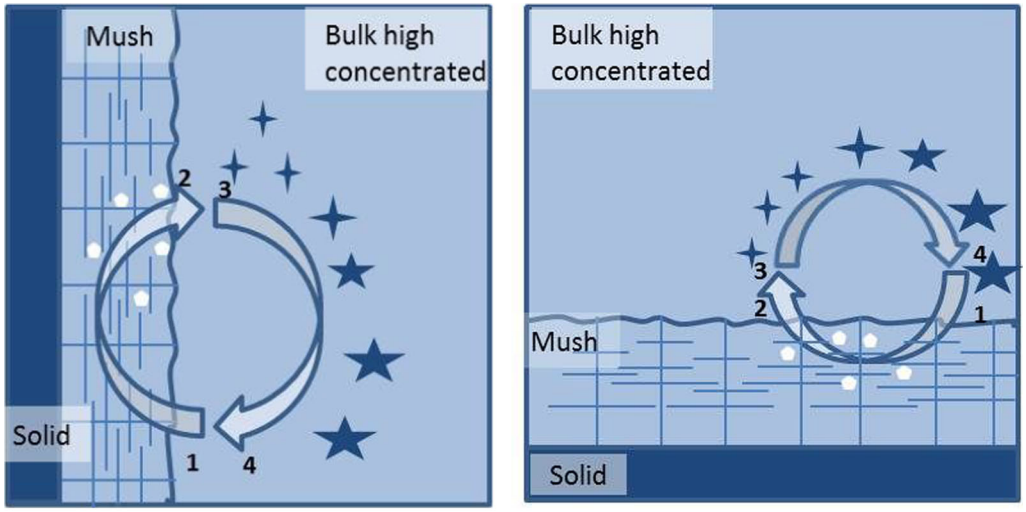

Fig. 14—Coupling mechanism at the origin of CET: 1-2 strong flow running through the mush transporting out dendrite fragments (white dots); 3-4 equiaxed growth and drag of the downward flow. If the vortex is sufficiently stable, the horizontal configuration can lead to freckle appearing; (*a*) vertical solidification front; (*b*) horizontal solidification front.

different growth rates. Results indeed indicate that the values of λ_1 and λ_2 decrease as the growth rate V increases, for a given concentration. Eqs. [6] and [7] present the relationship found for SCN-5 wt pct CTB, where k_1 and k_2 are constants:

$$\lambda_1 = k_1 V^{-0.25}, \quad [6]$$

$$\lambda_2 = k_2 V^{-0.46}. \quad [7]$$

These exponent values demonstrate that the dependency of the secondary dendrite arm spacing on the growth rate is stronger than the primary dendrite arm spacing, for the same concentration alloy.

Assuming a small cubic volume element Δx^3, the number of columnar primary arms (supposing they are uniformly distributed in the element) is $N_{d1} = \Delta x^2/\lambda_1^2$. The number of secondary arms F_2 growing perpendicularly to a single primary arm is equal to $4\Delta x/\lambda_2$. If we neglect the tertiary arms, the total number of dendrite arms $N_d = N_{d1} + N_{d2}$ existing in this volume element can be expressed by the following relation:

$$N_d \propto \Delta x^3 \left(\frac{1}{\lambda_1^2} \cdot \frac{4}{\lambda_2} \right). \quad [8]$$

By considering $\lambda_1 = 10^{-3}$ and $\lambda_2 = 10^{-6}$, which are common values for ammonium chloride, Eq. [8] gives a number density in the order of 10^{12} arms per m^3. As mentioned in Eqs. [5] through [7], λ_1 and λ_2 are closely related with G and V, therefore N_d can be related with G and V and the relation is shown in Eq. [9]:

$$N_d \propto G^{3/2} V \quad [9]$$

Using the relations from Eqs. [3] and [4], N_d is found to increase with the 7/2 power of the columnar front undercooling:

$$N_d \propto \Delta T_C^{7/2} \quad [10]$$

This equation expresses the fact that an increase in the velocity growth or undercooling will induce a huge increase of the number of dendrite arms, which theoretically can be broken and become dendrite's fragments susceptible to grow into equiaxed grains later. It can be noticed that N_d increases much faster with undercooling than the nucleation rate based on N (Eq. [2]), this because of the power 7/2 larger than 2, but also because $\Delta T_u \leq \Delta T_C$. Thus the fragmentation hypothesis presents a higher potential for the creation of equiaxed crystals (even neglecting tertiary dendrite arms) than the nucleation hypothesis where only a limited number of inoculants might exist.

Experiments demonstrate that fragmentation/detachment of secondary dendrites is more frequent in concentrated alloys under high growth rate.[27] The large velocity growth will provide a large tip undercooling and creates thinner secondary arms with finer arm neck, consequently these structures are more prone to remelt, than a coarser arm neck. Higher growth rate will also create larger number of secondary arms, thus the condition to enable detachment is increased.

Remelting, which can be at the origin of dendrite fragments is favored by the increase of the solid front velocity. When the solidification rate increases, the solutal buoyancy increases, due to more solute being rejected, this will bring about an intensification of the melt flow. This strong convection enhances the heat and mass transfer, brings more solute locally in the mushy

zone and induces remelting.

The formation of dendrite fragments in the mushy zone is only the beginning of the creation of equiaxed grains. Those fragments should be transported out of the mush into an undercooled zone. In this case, a strong flow would be beneficial. The stronger is the melt flow, the more likely the fragments will be transported out of the mushy zone.

Via a calculation of the Rayleigh (*Ra*) number, the association of the liquid height in the cell and flow magnitude can be accomplished.[21] For a higher liquid height a larger *Ra* number is obtained, respectively a more important flow is encountered. The flow KE evolution during the solidification, confirms that in the higher cell, the flow is stronger than in the lower cell (Figure 10). Thus the likelihood of importing a fragment from the mush out in the undercooled zone is much greater in the case of the higher cell. Figure 9 shows a good correlation with this theory. It can be seen that for large melt velocity equiaxed crystals always occurred (colorful points) and for small flow velocity equiaxed crystals are not present (kaki points). Considering the fragmentation theory, the strength of the melt flow can be correlated with the creation of equiaxed crystals as was experimentally observed by Paradies *et al.*[2] in their investigation on the convection influence on the fragmentation. It showed an increase of the fragmentation rate with the increase of the melt flow next to the mushy region.

D. *Final Assessment: Nucleation or Fragmentation as Source for equiaxed Grains and Mechanism of Creation of Equiaxed Grains*

Concerning the heterogeneous nucleation the seeding flow particle (20 μm polyamide particles coated with Rhodamine) can be considered as substrate. Solidification experiments with and without the seeding flow particles (Rhodamine-coated polyamide particle) were performed. A large amount of equiaxed crystals was noticed in both experiments without and with seeding particles. We did not count the number of equiaxed grains, we only evaluated area size covered by equiaxed crystals. If heterogeneous nucleation occurred on seeding particles, then much less equiaxed would have been observed during the experiments without seeding particles. This situation confirms in the balance that fragmentation is at the origin of equiaxed crystals, because fragmentation occurs independently of seeding particles.

The fact that the equiaxed crystals always appeared after a layer of columnar mush occurred at the cell's walls, and never prior to that, is another strong argument for the fragmentation theory. This assertion was also published by Montgomery and Incropera in their study of directional solidification of ammonium chloride.[12] They observed a maximum of dendrite's fragments at 2.5 mm mushy region growing at the lateral wall. The presence of columnar region seems to be a necessary condition for the creation of the first equiaxed crystals. Equiaxed crystals appear a few minutes after the start of columnar region at cell's walls. The equiaxed crystals were observed in both cases low cell and high cell, but their number, distribution in space and time was very different. This difference resulted in the final solidification type, mainly columnar in former case and predominantly equiaxed for the second.

Based on our experimental results and analysis, we propose a mechanism that couples the naturally driven flow with the equiaxed grain dynamics. This mechanism depicted schematically in Figure 14, can trigger a transition from a purely columnar to an equiaxed solidification (CET). Solutal convection cells are present along the mushy zone. At point 1, an ammonium chloride-rich flow penetrates the mushy zone and the columnar front continues to solidify. As the solidification takes place the liquid flowing through the mush becomes lighter. Due to this local change in the interdendritic composition, the liquidus temperature increases and remelting occurs. Consequently, dendrite fragments form in the mush. The flow will exit the mushy zone at point 2 carrying out dendrite's fragments. These fragments arriving in the undercooled and high concentrated bulk liquid will grow into equiaxed dendrites (Figure 14 point 3). Once they reach a certain size, the equiaxed crystals will descend (Figure 14 point 4). Due to the drag interaction the flow will be accelerated by the falling equiaxed crystals (Figure 14 point 3 to 4). In this manner, the full convection cell is strengthened, and the flow which renters the mush is now able to transport even more fragments out of the mushy zone. As follows, a coupling between the strength of flow and production equiaxed grains takes place. By this mechanism, the flow is accelerated as long as fragments are produced in the mushy region and as the concentration in the liquid bulk stays high enough. However, the acceleration of the flow is constrained by the mush permeability, and perhaps by a limited possible number of fragments created in the mush during solidification. As explained in Section IV–C, the fragmentation theory is constrained by the number of dendrite arms, which is indisputably extremely high but decreases with time as solid fraction increases in the mush.

This coupling mechanism can also explain the observations made by Montgomery and Incropera.[12] In the present experiments, a eutectic reaction does not take place, so the latent heat release cannot be at the origin of the first dendrite fragments. Nevertheless, local concentration changes in the interdendritic liquid take place and may cause remelting. Even if all stages for the creation of dendrite's fragments cannot be accounted for in current investigations, the fact that the number of equiaxed crystals starts to increase once the solutal convection becomes strong is a good indication that the coupling mechanism strongly correlates with flow behavior. In Reference 12 during vertical direct solidification (VDS) it was also observed that fragments reached a peak during transition from solutal fingers to channels, which means that the presence of strong solutal flow was beneficial in the formation of dendrite fragments. For horizontal direct solidification (HDS) the influence of the flow was more obvious as the thermal convection was the first source of fragments, but later, the water-rich interdendritic liquid was again

at the origin of the fragment production *via* salt fingering and channels. In our present investigations, the number of equiaxed crystals was indeed more important at the horizontally growing mush and always occurred initially along the horizontally growing mush. However, when channels occurred at the vertically growing mush, then the amount of equiaxed crystal reached a peak.

From the experimental observations it seems that the coupling mechanism occurs easier at the lateral mush (first equiaxed grains are always observed there), but the same mechanism can also occur at the bottom mush (Figure 14(b)). Along the lateral mush, the convection cells are relatively more stable and for this reason the coupling mechanism occurs with greater ease. It is necessary that the convection cell is relatively stable so that the flow enters and exits the mushy zone in the same region for a certain time until enough dendrite fragments are transported out of the mush. The strength of the flow at the mushy zone entry (point 1 in Figure 14) is a capital factor in the occurrence of this mechanism as it depends on how many fragments are transported out of the mush. The results shown in Figure 10 confirm this assertion and as for the predominantly equiaxed solidification (red curve) the point C has a higher flow velocity than point A on the black curve (mainly columnar solidification). This mechanism is fully verified, considering the fact that in the case of the higher cell, the flow was stronger than in the case of the lower cell at the moment when the very first equiaxed crystals occurred. If the vortex is sufficiently stable (points 3 to 4 in Figure 14), the equiaxed crystal falls can considerably strengthen the solutal convection. Remelting and/or low velocity front solidification can occur at the vicinity of point 2 (Figure 14(b)), giving rise to a freckle with its associated strong liquid jet driving away fragments far into the liquid bulk.

V. CONCLUSIONS

For the current experiments (9.5 cm liquid height) equiaxed crystals were generated in all cases for all concentrations from 27 to 31 wt pct.

1. The phenomena took place throughout the bulk melt and lasted for a long time (between 30 and 54 minutes). For the lower concentration group (27 to 28 wt pct), even chimneys appeared and the amount of equiaxed grains was enormous.
2. The flow kinetic energy showed a clear correlation between the occurrence of the equiaxed crystals and the flow; the onset of equiaxed crystals is always accompanied by an increase of the flow kinetic energy.
3. A coupling mechanism between the flow and the creation of equiaxed crystals was proposed in order to explain the occurrence of CET. The strength of the naturally driven flow at the mushy zone entrance is an important factor in the coupling mechanism and has been confirmed by the present results. In this mechanism, the number of equiaxed crystals is increased by the number of fragments driven out of the mushy region by the interdendritic flow. The solutal, convective flow is strengthened by the falling equiaxed crystals dragging in the liquid bulk. A coupling can occur if the bulk flow and the interdendritic flow are part of a single circulation cell. This mechanism can thus generate freckles at horizontal solidification fronts, and trigger a CET transition.

ACKNOWLEDGEMENTS

Open access funding provided by Montanuniversity Leoben.

REFERENCES

1. J.A. Dantzig, M. Rappaz, *Solidification*, EPFL Press, 2009.
2. C.J. Paradies, R.N. Smith, and M.E. Glicksmann: *Metall. Mater. Trans. A*, 1997, vol. 28A, pp. 875–83.
3. K.A. Jackson, J.D. Hunt, D.H. Uhlmann, and T.P. Seward: *Trans. TMS-AIME*, 1966, vol. 236, pp. 149–58.
4. T. Campanella, C. Carbon, and M. Rapaz: *Metall. Mater. Trans. A*, 2004, vol. 35A, pp. 3201–10.
5. M.C. Flemings: *Solidification Processing*, 1974.
6. K. Dragnevski, A.M. Mullis, D.J. Walker, and R.F. Cochrane: *Acta Mater.*, 2002, vol. 50, pp. 3743–55.
7. J. Pilling and A. Hellawell: *Metall. Mater. Trans. A*, 1996, vol. 27A, p. 229.
8. R.H. Mathiesen, L. Arberg, P. Bleuet, and A. Somogyi: *Metall. Mater. Trans. A*, 2006, vol. 37A, pp. 2515–24.
9. D. Ruvalcaba, R.H. Mathiesen, D.G. Eskin, L. Arnberg, and L. Katgerman: *Metall. Mater. Trans. B*, 2009, vol. 40B, pp. 312–16.
10. C. Beckermann: *JOM*, 1997, vol. 49, pp. 13–17.
11. A. Kumar and P. Dutta: *J. Phys D*, 2008, vol. 41, pp. 1–9.
12. W.C. Mongomery and F.P. Incropera: *Exp. Heat Transf.*, 1998, vol. 11, pp. 59–86.
13. Ch.A. Gandin: *Acta Mater.*, 2000, vol. 48, pp. 2483–2501.
14. M.A. Martorano, C. Beckermann, and Ch.A. Gandin: *Metall. Mater. Trans. A*, 2003, vol. 34A, pp. 1657–74.
15. J.D. Hunt: *Mater. Sci. Eng.*, 1984, vol. 65, pp. 75–83.
16. D.J. Browne: *ISIJ Int.*, 2005, vol. 45, pp. 37–44.
17. T. Sivarupan, C. H. Caceres, and J. A. Taylor: *Metall. Mater. Trans. A*, 2013 on line.
18. D. Ma, W. Xu, S.C. Ng, and Y. Li: *Mat. Sci. Eng. A*, 2005, vol. 390, pp. 52–62.
19. G. Hansen, A. Hellawell, S.Z. Lu, and R.S. Steube: *Metall. Mater. Trans. A*, 1996, vol. 27A, pp. 569–81.
20. M. Stefan-Kharicha, A. Kharicha, M. Wu, and A. Ludwig: *Fluid Dyn. Res.*, 2014, vol. 46, pp. 1–21.
21. A. Kharicha, M. Stefan-Kharicha, A. Ludwig, and M. Wu: *Metall. Mater. Trans. A*, 2013, vol. 44A, pp. 650–60.
22. A. Kharicha, M. Stefan-Kharicha, A. Ludwig, and M. Wu: *Metall. Mater. Trans. A*, 2013, vol. 44A, pp. 661–68.

23. W. Oldfield: *Trans. ASM*, 1966, vol. 59, pp. 945–61.
24. J. D. Hunt: *Solidification and Casting of Metals,* Metals Society London, 1979, pp. 1-3.
25. W. Kurz and J.D. Fisher: *Acta Metall.*, 1981, vol. 29, pp. 11–20.
26. H. Kaya, E. Cadirli, K. Keslioglu, and N. Marasli: *J. Cryst. Growth*, 2005, vol. 276, pp. 583–93.
27. T. Sato, W. Kurz, and K. Ikawa: *Trans. Jpn. Inst. Metals*, 1987, vol. 28, pp. 1012–21.